Optics Communications 454 (2020) 124520

Contents lists available at ScienceDirect

Optics Communications

journal homepage: www.elsevier.com/locate/optcom

Performance evaluation of direct-detection coherent receiver array for free-space communications with full-link simulation

Zhaoxin Yu [a,b], Rujun Cai [a,b], Zhihang Wu [a], Hongwei He [a], Hexin Jiang [a,b], Xianglian Feng [a,b], Anrui Zheng [a,b], Junfan Chen [a,b], Shiming Gao [a,b,*]

[a] Centre for Optical and Electromagnetic Research, State Key Laboratory of Modern Optical Instrumentation, Zhejiang University, Hangzhou 310058, China
[b] Ningbo Research Institute, Zhejiang University, Ningbo 315100, China

ARTICLE INFO

Keywords:
Free-space optical communications
Spatial diversity
Single-photodetector direct-detection coherent receiver
Full-link simulation model

ABSTRACT

Performance of the direct-detection coherent receiver array for free-space optical (FSO) communications is evaluated with a full-link simulation model. This FSO full-link model (from the transmitter to the receiver) is established based on the phase screen method and the coupling theory by considering the amplitude fading and the phase distortion caused by atmospheric turbulence. Via full-link simulation, bit error rates are evaluated using maximum ratio combining and equal gain combining algorithms based on single-photodetector direct-detection coherent receiver array with different receiver numbers. The improvement of spatial diversity is numerically demonstrated by comparing with the single receiver.

1. Introduction

Free-space optical (FSO) communications have attracted significant attentions in military and aerospace fields [1]. Due to its advantages of high transmission rate, large available bandwidth, high security and strong anti-interference ability, FSO communications can be used for the links between satellites, aircrafts, ships and other space or ground platforms [2,3]. Currently, laser communications relay demonstration (LCRD) has been successfully achieved by NASA to enable optical wireless communications of satellites, deep space optical terminals and ground, and it is scheduled to formally launch in 2019 [4]. Although FSO communications can offer these advantages, laser carriers are susceptible to weather condition and atmospheric turbulence, which seriously degrades the quality of received signals. The atmospheric turbulence leads to wavefront distortions, intensity fading and phase fluctuations of laser carriers, which reduces the signal-to-noise ratio (SNR) of receivers and increases the reception bit error rate (BER) [5,6].

Multi-level coherent modulation formats such as quadrature phase shift keying (QPSK) and quadrature amplitude modulation (QAM), which make full use of the amplitude and phase variation of the optical carriers, have highly spectral efficiency and are the effective way to improve the transmission capacity [7]. However, these multi-level coherent modulation formats require higher SNR to ensure the reception BER. Recently, diversity techniques have become an effective way to improve the reception SNR in FSO coherent communication systems [2]. Diversity technology usually transmits the same information or channel coded information in different dimensions of the optical carriers, and increases redundancy of the system by using uncorrelated received signals, so as to improve the ability against fading and reliability of the system [8]. As the most commonly used diversity technique, spatial diversity using receiver array adopts multiple receivers with fixed distance to achieve better performance than a single large-aperture receiver with the same coupling efficiency [9]. Moreover, multiple-input multiple-output (MIMO) channel with multiple transmitters and multiple receivers can be developed to further improve the system capacity and reliability [10]. In spatial diversity, receiver array is the key element. Although coherent optical receivers can suppress background noises and provide a 3-dB detection improvement [11], they are not enough to defense the atmospheric turbulence and they are also quite complex and expensive. Compared to the conventional balanced-detection coherent receivers, single-photodetector direct-detection (SPD-DD) coherent receiver are more competitive due to its simple structure and low cost [12].

In the past, most of the contributions only focused on the influence of the atmospheric channel on the signal quality [13–17], the coupling efficiency [16–18] and detection noise are not included. This leads to inaccurate performance evaluation of spatial reception, because the turbulence influence, coupling effect and detection noise of multi-channel signals will superimpose on each other and deteriorate the signal quality. In order to solve this problem, the influence along the full FSO link should been taken into account. The simulation model of the full link, from the transmitter, atmospheric channel, coupling,

* Corresponding author at: Centre for Optical and Electromagnetic Research, State Key Laboratory of Modern Optical Instrumentation, Zhejiang University, Hangzhou 310058, China.
E-mail address: gaosm@zju.edu.cn (S. Gao).

https://doi.org/10.1016/j.optcom.2019.124520
Received 14 May 2019; Received in revised form 11 August 2019; Accepted 5 September 2019
Available online 7 September 2019
0030-4018/© 2019 Elsevier B.V. All rights reserved.

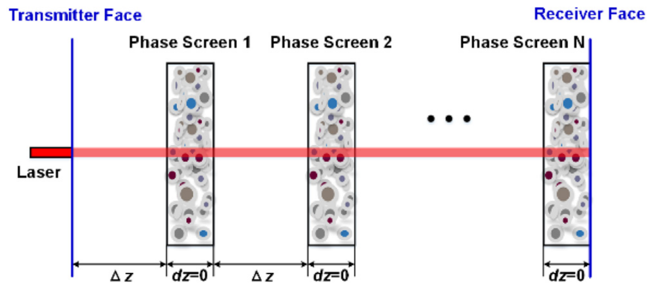

Fig. 1. Schematic description of the atmospheric turbulence channel simulation using phase screens.

and reception, need to be established. In this paper, we establish the FSO full-link model and study the improvement of diversity reception in FSO coherent communication systems with the SPD-DD receiver array. The relationship between SNR and BER is taken as an index to evaluate SPD-DD receiver array with different combining algorithms. In Section 2, we establish the simulation model for the full FSO link, including atmospheric turbulence model, coupling model and diversity reception scheme. In Section 3, the process of laser carriers propagating through a FSO link is analyzed and the performance improvement of the SPD-DD receiver array is verified. In Section 4, the conclusion is drawn.

2. FSO full-link simulation model

2.1. Transmission in atmospheric turbulence channel

In FSO communication systems, atmospheric turbulence will cause amplitude fading and phase distortion, which seriously affect the signal quality. In the past, a variety of theoretical models of atmospheric turbulence distribution have been established to evaluate the influence of atmospheric channel on the SNR and BER of the received signal, such as Gamma–Gamma model and log-normal model. However, these analytical methods can only analyze the impact caused by the atmospheric turbulence. As important parts of the full link, the impact of transmitter and receiver should also be evaluated. In order to analyze the improvement of reception performance by spatial diversity, the evolution of the laser carrier in the full FSO link need to be simulated.

Here, the phase screen method is selected for physical modeling and numerical simulation of the atmospheric channel [13–16], where the phase distribution due to the turbulence is obtained by the power spectral density function in the power spectral inversion method. Fig. 1 shows the process of the laser beam propagating through the phase screen model, which is constructed by power spectral inversion method. A section of the atmospheric medium is cut into several small segments with an adjacent distance of Δz. The vacuum propagation and the atmospheric turbulence phase perturbation are considered independently in each segment, which is equivalent to the vacuum propagation of the laser over a distance of Δz and the phase changes is produced on a phase screen without considering the thickness. We can simulate the changes of the optical field through the atmospheric turbulence channel by superimposing several equal-distance phase screens under the premise of specifying the distribution of the incident optical field.

Assuming that the phase change caused by the ith phase screen is $\phi_i(x, y, \Delta z)$, the change of the optical field $U(r, z)$, after the propagation of the ith distance, can be expressed as [15]:

$$U(x, y, z + \Delta z) = F^{-1}\{F[U(x, y, z)]\exp(\frac{jq^2\Delta z}{2k^2})\}\phi_i(x, y, \Delta z) \tag{1}$$

where $F(\cdot)$ represents a two-dimensional Fourier transform, q denotes the spatial frequency and k is the wavenumber. Using the iterative process, the output optical field with an arbitrary propagation distance can be calculated.

In Eq. (1), the phase change $\phi_i(x, y, \Delta z)$ caused by the phase screen directly affects the output optical field. The phase introduced by the ith phase screen can be written in the form of Fourier series:

$$\phi_i(x, y, \Delta z) = \sum_{n=-\infty}^{\infty}\sum_{n=-\infty}^{\infty} c_{n,m}\exp[j2\pi(f_{x_n}x + f_{y_m}y)] \tag{2}$$

where f_{x_n} and f_{y_m} are the spatial frequencies in the x and y directions, respectively, and $c_{n,m}$ are the coefficients of Fourier series, which are random numbers satisfying the Gaussian distribution. The mean value of the Gauss function is zero, and the variance is shown as:

$$\left\langle |c_{n,m}|^2 \right\rangle = \Phi_\phi(f_{x_n}, f_{y_m})\Delta f_{x_n}\Delta f_{y_m} \tag{3}$$

where Δf_{x_n} and Δf_{y_m} represent the grid size on the plane, and $\Phi_\phi(f_{x_n}, f_{y_m})$ is the spatial power spectral density. Using the modified von Kármán spatial power spectral density and converting f_{x_n} and f_{y_m} to θ and f in polar coordinates, one can get the following equation [16]:

$$\Phi_\phi(k) = 0.033C_n^2\frac{\exp(-k^2/k_m^2)}{(k^2 + k_0^2)^{11/6}} \tag{4}$$

where $k = 2\pi f, k_0 = 2\pi/L_0, k_m = 5.92/l_0, C_n^2$ is the atmospheric refraction-index structure parameter, L_0 and l_0 are the outer and inner scales of the turbulence, respectively.

Although the atmospheric turbulence changes in real time, the fluctuation of the atmospheric refractive index is a slowly changing random process for spatial laser signals. According to Taylor's "frozen turbulence" hypothesis [17], the change of the atmospheric turbulence at a given location over time can be interpreted as moving it within the phase screen with the average wind speed. It means that the changes of time will be manifested in the displacement between the relative static atmospheric turbulence distribution and the laser beam. The received aperture chosen in the case of long-distance transmission is relatively small. Correspondingly, the aperture smoothing effect has little influence and is not discussed here.

2.2. Coupling from free space to an optical fiber

Besides the fading effect of the atmospheric turbulence, the coupling efficiency from free space to the optical fiber will also affect the received signals. Traditionally, the receiving devices is based on single-mode fiber (SMF) and the mode field diameter of the SMF is about 10 μm, which greatly limits the anti-interference ability when suffering from atmospheric turbulence [18]. The coupling efficiency with multimode fiber (MMF) is effectively improved due to its large mode field diameter of more than 50 μm, but it is hardly compatible with the traditional SMF-based communication technology. In practical applications, the MMF can be used to improve spatial coupling efficiency, and then coupled into the SMF by adopting gradient-index (GRIN) lens to control the mode field diameter and divergence angle [19]. As shown in Fig. 2, the free-space light converges through the reception lens, and an Airy pattern with a radius of ω_1 is generated on the back focal plane, where U_{if} represents its optical field distribution. A MMF is placed on the focal plane and coupled with the spatial light, where U_f and ω_0 represent the mode field distribution and mode field radius of the fiber.

Here we assume that the optical carrier over long-distance propagation is distributed as a plane wave for calculation convenience, the process of propagation and focus is performed by Fresnel diffraction integral method [20]. The coupling efficiency η is defined as the ratio of the optical power incident on the reception plane to the optical power coupled into the MMF [21]:

$$\eta = \sum_{n=1}^{m}\eta_n \tag{5}$$

$$\eta_n = \frac{\left|\iint U_{if}^* U_{nf}\,ds\right|^2}{\iint \left|U_{if}\right|^2 ds \iint \left|U_{nf}\right|^2 ds} \tag{6}$$

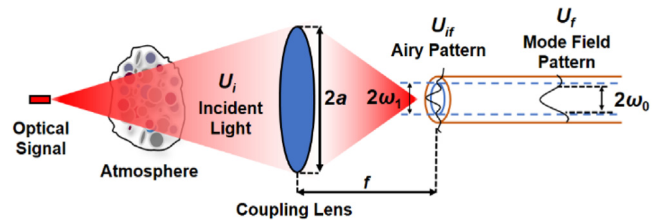

Fig. 2. Schematic diagram of the coupling from free space to a fiber through thin lens focusing.

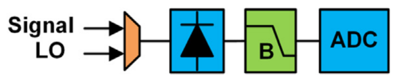

Fig. 3. Schematic diagram of the SPD-DD coherent receiver.

where m is the number of modes held by the MMF, η_n is the coupling efficiency of the nth mode of MMF, and U_{nf} is the back-propagation mode field of the nth mode of the MMF in the aperture plane, which is normalized as $\iint \left|U_{nf}\right|^2 ds = 1$.

2.3. SPD-DD coherent receiver

The SPD-DD coherent receiver can be implemented based on the structure shown in Fig. 3. This scheme eliminates the use of phase-diverse optical hybrid and balanced photodetectors [22]. The signal coupled from free space is mixed with a high-power frequency-offset local oscillator (LO) and impinges upon the photodetector. After sampled and analog–digital converted by an analog-to-digital converter (ADC), the signal is then processed by digital signal processing (DSP) based on Kramers–Kronig relation to reconstruct the complete mixing optical field.

Assuming the complex envelope of LO light and signal are $E_{LO}(t)$ and $E_{signal}(t)\exp(-j2\pi f_{IF}t)$, respectively, the f_{IF} is the frequency difference between them. The mixing optical field can be expressed as

$$E(t) = E_{LO}(t) + E_{signal}(t)\exp(-j2\pi f_{IF}t) = |E(t)|\exp[i\varphi(t)] \tag{7}$$

The amplitude of mixing optical field can be directly detected by a single photodetector:

$$|E(t)| = k\sqrt{I(t)} \tag{8}$$

The coefficient k is determined by the intrinsic impedance, the effective area and responsivity of the detector, and it can be normalized to 1. The power of LO is set much larger than that of signal to ensure $E(t)$ is the minimum phase signal, then the phase of mixing optical field can be obtained by Hilbert transfer based on Kramers–Kronig relations [12,23]

$$\varphi(t) = F^{-1}\left\{\frac{j}{2} sign(\omega) F\left\{\ln|I(t)|\right\}\right\} \tag{9}$$

where F and F^{-1} represent Fourier transform and inverse Fourier transform, respectively. $sign(\omega)$ is sign function

$$sign(\omega) = \begin{cases} -1, & \omega < 0; \\ 0, & \omega = 0; \\ 1, & \omega > 0. \end{cases} \tag{10}$$

Since the changing rate of LO is slower than that of high-speed DSP, it can be further assumed that the complex envelope of LO is a constant with the central symmetry during signal reconstruction, which can be estimated by the direct current (DC) component of the detected optical field's complex envelope:

$$\hat{E}_{LO} = \overline{|E(t)|\exp[j\varphi(t)]} \tag{11}$$

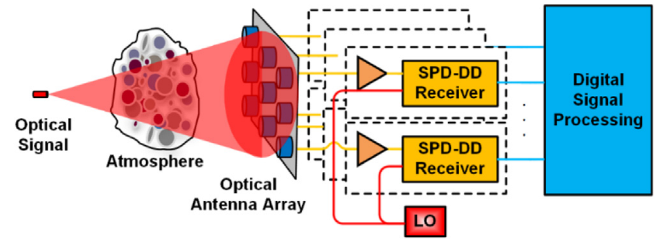

Fig. 4. Schematic diagram of the SIMO-FSO communication system.

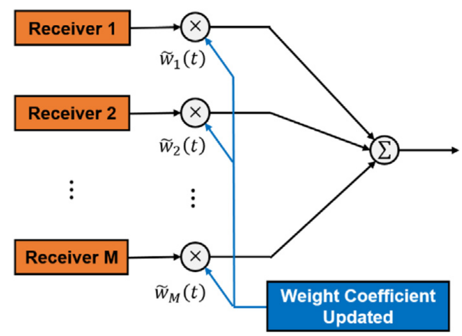

Fig. 5. Coherent combining model for the spatial diversity reception based on receiver array.

Finally, the optical field of signal can be represented as

$$\hat{E}_{signal}(t) = \left[|E(t)|\exp[j\varphi(t)] - \hat{E}_{LO}\right] \cdot \exp(j2\pi f_{IF}t) \tag{12}$$

2.4. Diversity reception scheme based on receiver array

After the optical carrier is launched from the transmitter, it propagates through the atmospheric turbulence channel, which results in phase distortion, signal drift, scintillation effect and other harmful effects. Therefore, effective methods should be adopted at the reception end to reduce the signal fading. Diversity reception is to transmit the same information through mutually independent paths and utilizes multiple sets of mutually independent fading signals to obtain greater signal power and higher SNR at the reception terminal [24].

As a common spatial diversity system, the single-input multiple-output (SIMO) model is shown in Fig. 4, in which the receivers are staggered spatially and the paths from the transmitter to the receivers are independent of each other. In the receiver array, each signal propagating through the fading channel independently is coupled into the corresponding fiber by each single optical antenna (served by a single optical lens or an optical system) and then sent to receivers. After compensation and reconstruction, a suitable combining algorithm will be selected to implement the delay alignment, phase alignment and signal combining through DSP for the signals detected by each receiver. The combining model for receiver array composed of M receivers is shown in Fig. 5.

Fig. 6 shows the DSP process. The baseband signal is first reconstructed using Kramers–Kronig relations as shown in Eqs. (7)–(12) before down-sampling. After that, the identical DSP is carried out for each signal from the receiver array. The twofold oversampled signal is resampled to the symbol rate after recovering the timing clock. Constant modulus algorithm (CMA) is employed to equalize the linear impairments. Viterbi–Viterbi phase estimation (VVPE) and blind phase search (BPS) algorithms are adopted to alleviate the residual frequency offset and to compensate the phase noise in laser carriers.

As for phase alignment, it can be performed before frequency offset establishment, phase noise compensation and signal reconstruction, so as to reduce the complexity of the whole algorithm. Choosing a branch

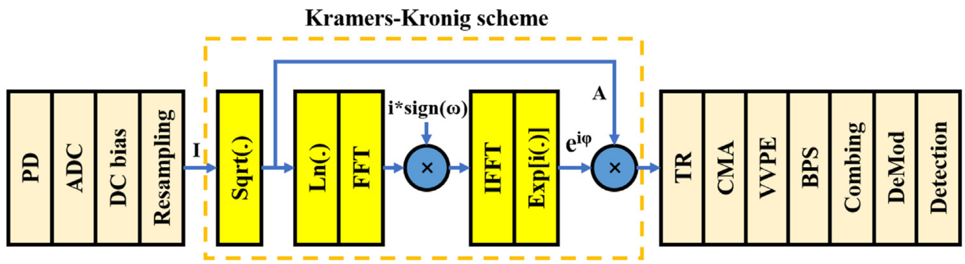

Fig. 6. The flowchart of the DSP process in the receiver array.

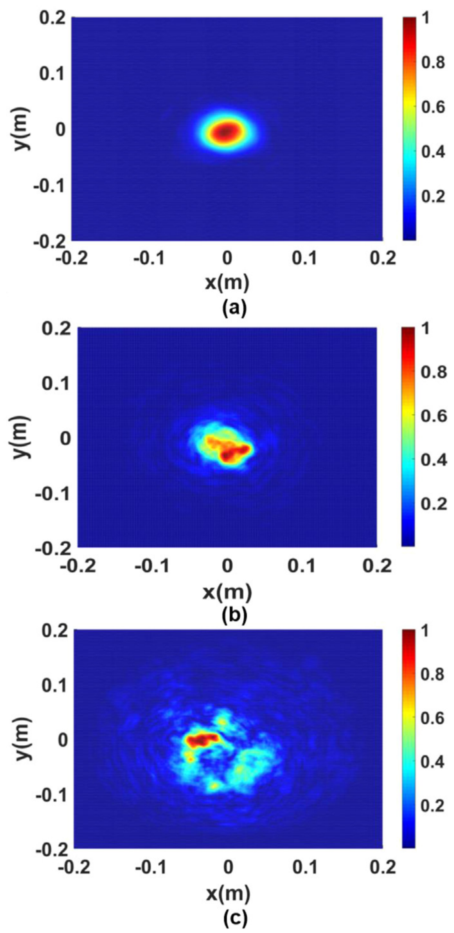

Fig. 7. Received optical field distributions when the atmospheric refraction-index structure parameters C_n^2 are (a) 5.0×10^{-16} $m^{-2/3}$, (b) 5.0×10^{-15} $m^{-2/3}$ and (c) 5.0×10^{-14} $m^{-2/3}$, respectively.

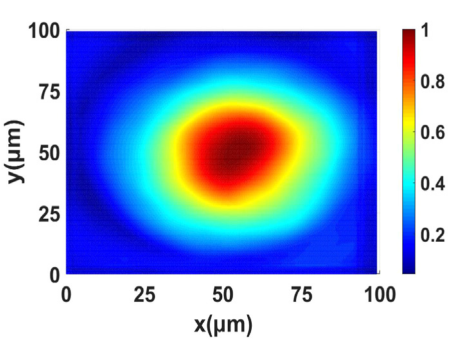

Fig. 8. Airy spot optical field distributions after normalization when the C_n^2 takes value of 5.0×10^{-15} $m^{-2/3}$ and the transmission distance is 1 km.

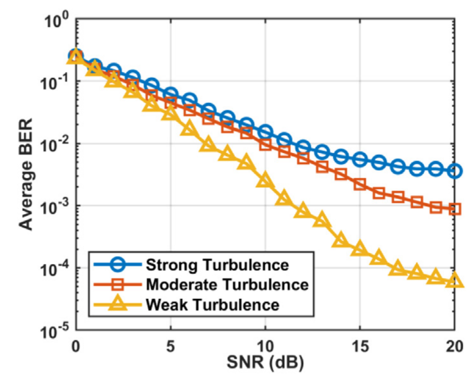

Fig. 9. Comparison of BER in SPD-DD receivers under different strengths of atmospheric turbulence.

signal with the largest SNR as reference signal x_{ef}, the relative phase $\varphi_{relative}$ of each branch signal x_{in} can be estimated as

$$\varphi_{relative} = \arg(x_{ef} \cdot x_{in}^{*}) \tag{13}$$

After subtracting the relative phase from branch signals, coherent combining can be performed.

The combining process can be implemented in a variety of ways with different complexities and performances, and the simplest technique is linear combining, which is represented as

$$y = \sum_{i=1}^{M} \widetilde{w}_i(t) x_i(t) \tag{14}$$

where signals detected by each branch expressed as $x_i(t) = a_i(t) + n_i(t), a_i(t)$ is the signal and $n_i\ (t)$ is the noise. The weight coefficient $\widetilde{w}_i(t) = w_i(t)e^{j\theta_i(t)}$, where the real number $w_i(t)$ represents the weight of each branch in the combining process and the phase factor $e^{j\theta i(t)}$ indicates the phase alignment of each branch to enable coherent superposition. The combining process is non-coherent without phase alignment, each branch preserves the random phase jitter from the atmospheric channel, which is equivalent to optical reception signal by one receiver with a large aperture. It means that the atmospheric fading effect has not been effectively alleviated.

Assume that the responsivity and the noise of each receiver are the same. In the actual reception process, the phase between receivers is different due to the interference of the atmospheric turbulence and other factors, so the combining algorithm will directly determine the gain of the spatial diversity. Typical linear combining algorithms include selection combining (SC), maximal-ratio combining (MRC) and equal-gain combining (EGC) [25,26].

In the SC algorithm, the combining device directly selects the branch signal with the highest SNR for signal reconstruction, which is equivalent choosing the weight coefficient of the maximum power signal being 1 and the others being 0 in Eq. (13). In this algorithm, only one signal enters the final demodulator and the phase alignment can be left out, which reduces the complexity of the receiver but does

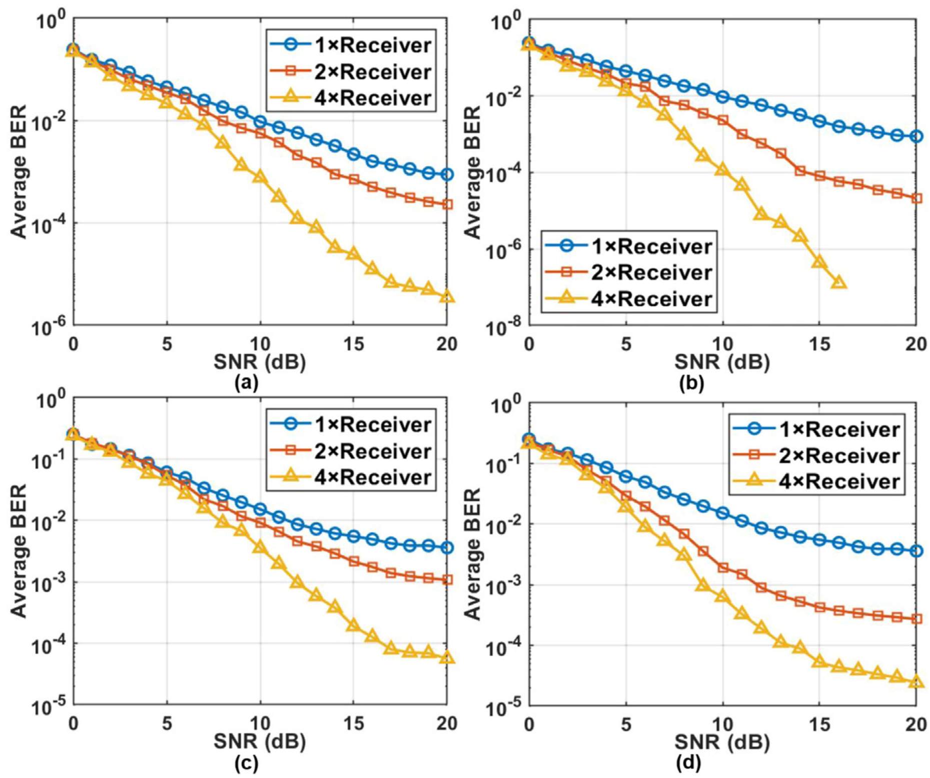

Fig. 10. BERs of the receivers with single, two and four apertures when (a) C_n^2 takes the value of 5.0×10^{-15} $\mathrm{m}^{-2/3}$ and the EGC algorithm is adopted, (b) C_n^2 takes the value of 5.0×10^{-15} $\mathrm{m}^{-2/3}$ and the MRC algorithm is adopted, (c) C_n^2 takes the value of 5.0×10^{-14} $\mathrm{m}^{-2/3}$ and the EGC algorithm is adopted, (d) C_n^2 takes the value of 5.0×10^{-14} $\mathrm{m}^{-2/3}$ and the MRC algorithm is adopted.

not achieve the maximum diversity gain. Relative to MRC and EGC, the SC algorithm is too simple to significantly improve the reception performance, which will not be further discussed in our following numerical simulation [26].

In the MRC algorithm, appropriate weight coefficients are selected to maximize the SNR of the combined output signal for the multi-aperture receiver. After phase alignment, the SNR of the combined output signal from the receiver array is expressed as

$$\gamma = \frac{y^2}{N_{total}} = \frac{1}{N_0}\frac{\left[\sum_{i=1}^{M} w_i(t)x_i(t)\right]^2}{\sum_{i=1}^{M} w_i(t)} \tag{15}$$

where N_0 is the power spectrum density of the receiver noise. Deriving Eq. (14) or using the Cauchy–Schwartz inequation, the SNR of the output signal reaches the maximum when $w_i(t) = x_i^2/N_0$, which is expressed as

$$\gamma = \sum_{i=1}^{M}\frac{x_i^2(t)}{N_0} = \sum_{i=1}^{M}\gamma_i \tag{16}$$

The maximum output SNR is the sum of each receiver.

In the EGC algorithm, the weight coefficients are set to be $\widetilde{w}_i(t) = e^{j\theta_i(t)}$ to simplify the combining process. When the quality of each branch is quite different, the combined output signal will get worse. This problem can be solved by the MRC algorithm, which dynamically assigns the weights of all the branches. The MRC algorithm can obtain the maximum gain in principle, but it needs to obtain the SNR of each branch in real time.

3. Results and discussion

Using the established phase screen model, the propagation and evolution of the laser beam in the atmospheric channel can be simulated. The laser carrier is supposed as a Gauss beam and the simulation parameters are as follows: the wavelength λ is 1550 nm, the propagation distance L is 1 km, which is divided into 10 segments with each interval of 100 m and the phase screen is set in the middle of each segment, the outer scale of turbulence L_0 and inner scale of turbulence l_0 are 100 m and 0, respectively, the grid interval of the phase screen is 10^{-3} m, the size of the phase screen is 0.4 m × 0.4 m. At the reception terminal, when C_n^2 takes the values of 5.0×10^{-16} $\mathrm{m}^{-2/3}$, 5.0×10^{-15} $\mathrm{m}^{-2/3}$ and 5.0×10^{-14} $\mathrm{m}^{-2/3}$, respectively, the normalized optical field distributions after propagating through the atmospheric channel are shown in Fig. 7. It can be seen that the diffusion and distortion of the optical field become more obvious as the turbulence changes from weak to strong, which will directly affect the reception SNR and BER.

The atmospheric turbulence link is simulated by the above phase screen method. Considering a 20 Gb/s QPSK signal, the signal passing through the turbulent channel is simulated based on "frozen turbulence" hypothesis. The wind speed is set to be 10 m/s and 10^6 symbols of data are inserted each time when a grid is moved. And then, the optical signal from the atmospheric turbulence link is coupled into the optical fiber via optical lens.

For the condition that λ is 1550 nm, $2\omega_0$ is 50 μm, $2a$ is 0.2 m and f is 0.4 m, the optical field distribution of the received signal is shown in Fig. 7(b). The optical field of the Airy spot, which has been converged by the lens, is shown in Fig. 8. The mode field radius of the SMF is set 5 μm and the coupling efficiency of MMF to the SMF is calculated to be around 40%. However, in order to analyze the performance of diversity reception, the received signals are normalized to ensure that the total average received optical power of the single receiver or the receiver array is consistent.

For the 20 Gb/s QPSK signals with a long transmission distance of 20 km, the normalized intensity scintillation and phase fluctuation can be obtained by the full FSO link simulation when the refractive-index structure parameter C_n^2 is 5.0×10^{-16} $\mathrm{m}^{-2/3}$, 5.0×10^{-15} $\mathrm{m}^{-2/3}$ and

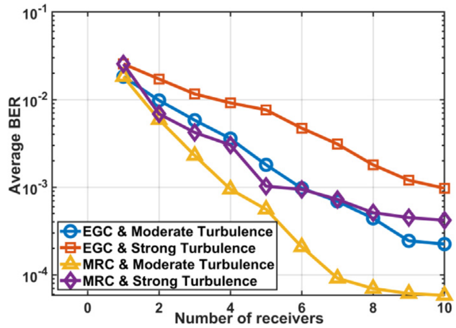

Fig. 11. BER versus the number of receivers with the SNR of 8 dB.

5.0×10^{-14} $m^{-2/3}$, corresponding to weak turbulence, moderate turbulence and strong turbulence, respectively. The wavelength of LO is 1550.08 nm, where 0.08 nm corresponds to a 10 GHz frequency offset from 1550 nm, and the LO power is set to 1.2 times the maximum value of the signal power to make sure the minimum-phase condition is fulfilled. After mixing the LO and received signal, the DSP is operated similar to that in Fig. 6 without signal combining here. Under different parameters conditions, 1000 sets of data are recorded with the length of 1×10^6 symbols to calculate the BER respectively, and then to calculate the average BER. Fig. 9 depicts the variation of the BER versus the SNR for the SPD-DD receiver. One can find that the performance of the SPD-DD receiver can be influenced by different strengths of the atmospheric turbulence.

Fig. 10 shows the variation of the BER versus the SNR for multi-aperture receivers. Comparing and analyzing the results of the single receiver, the two-aperture receiver array and the four-aperture receiver array, it can be found that the reception performance can be effectively improved by introducing multi-aperture receiver array under different atmospheric turbulences and different algorithms. The EGC algorithm is much simpler than the MRC algorithm since the weight coefficients are the same. However, the performance of the EGC algorithm is worse, especially when the number of the receivers is small. The MRC algorithm can significantly improve the performance of the receivers, but it requires the SNR of the received signals to allocate the weight coefficients in real time. They can be selected according to the real signal quality to meet the reception requirement. Under the influence of the atmospheric turbulence, the severe signal drift and distortion caused by atmospheric turbulence is difficult to be fully compensated by the DSP. Therefore, the BER results of the receiver seem to saturate at high SNR values. When the original signal has high quality, the saturation becomes more obvious. The stronger the turbulence is, the more obvious the BER saturation effect is.

Fig. 11 shows the variation of BER with the number of the SPD-DD receivers for various turbulence conditions with the average SNR of 8 dB. It can be observed that all the BERs reduce as the number of the receivers increases under different turbulence levels.

4. Conclusion

A FSO full-link simulation model has been established and it has been used to evaluate the spatial diversity reception based on SPD-DD coherent receiver array with QPSK signals. All the effects including the laser carrier propagating in the atmospheric channel, coupling into the optical fiber, receiving by the receiver array are concerned. The process of Gaussian beam passing through atmospheric turbulence is analyzed using the phase screen model. The coupling process is analyzed by coupling theory. By choosing suitable combining algorithms, the reception SNR and BER can be effectively improved by using spatial diversity based on the receiver array compared to the single SPD-DD receiver.

Acknowledgments

This work was supported in part by the National Natural Science Foundation of China (Grant No. 61875172) and the Zhejiang Provincial Natural Science Foundation of China (Grant No. LD19F050001).

References

[1] M.A. Khalighi, M. Uysal, Survey on free space optical communication: A communication theory perspective, IEEE Commun. Surv. Tutor. 16 (2014) 2231–2258.
[2] V.W.S. Chan, Free-space optical communications, J. Lightwave Technol. 24 (2007) 4750–4762.
[3] X. Yi, Z. Liu, P. Yue, Optical scintillations and fade statistics for FSO communications through moderate-to-strong non-Kolmogorov turbulence, Opt. Laser Technol. 47 (2013) 199–207.
[4] D.J. Israel, B.L. Edwards, J.W. Staren, Laser communications relay demonstration (LCRD) update and the path towards optical relay operations, in: IEEE Aerospace Conference, 2017, pp. 1-6.
[5] H. Yao, X. Ni, C. Chen, B. Li, X. Zhang, Y. Liu, S. Tong, Z. Liu, H. Jiang, Performance of M-PAM FSO communication systems in atmospheric turbulence based on APD detector, Opt. Express 26 (2018) 23819–23830.
[6] H. Yao, X. Ni, C. Chen, X. Feng, X. Liu, Z. Liu, S. Tong, H. Jiang, Performance analysis of MPSK FSO communication based on the balanced detector in a fiber-coupling system, IEEE Access 7 (2019) 84197–84208.
[7] G. Li, Recent advances in coherent optical communication, Adv. Opt. Photonics 1 (2009) 279–307.
[8] D.J. Geisler, T.M. Yarnall, M.L. Stevens, C.M. Schieler, B.S. Robinson, Multi-aperture digital coherent combining for free-space optical communication receivers, Opt. Express 24 (2016) 12661–12671.
[9] M.A. Khalighi, N. Schwartz, N. Aitamer, S. Bourennane, Fading reduction by aperture averaging and spatial diversity in optical wireless systems, J. Opt. Commun. Netw. 1 (2009) 580–593.
[10] A.J. Paulraj, D.A. Gore, R.U. Nabar, H. Bolcskei, An overview of MIMO communications - a key to gigabit wireless, Proc. IEEE 92 (2004) 198–218.
[11] J.R. Barry, E.A. Lee, Performance of coherent optical receivers, Proc. IEEE 78 (1990) 1369–1394.
[12] A. Mecozzi, C. Antonelli, M. Shtaif, Kramers–Kronig coherent receiver, Optica 3 (2016) 1220–1227.
[13] M.R. Chatterjee, F.H.A. Mohamaed, Investigation of profiled beam propagation through a turbulent layer and temporal statistics of diffracted output for a modified von Karman phase screen, Proc. SPIE 8971 (2014) 897102.
[14] V.S.R. Gudimetla, R.B. Holmes, T.C. Farrell, J. Lucas, Phase screen simulations of laser propagation through non-Kolmogorov atmospheric turbulence, Proc. SPIE 8038 (2011) 803808.
[15] E.M. Whitfield, P.P. Banerjee, J.W. Haus, Propagation of Gaussian beams through a modified von Karman phase screen, in: Laser Communication and Propagation through the Atmosphere and Oceans, Vol. 8517, 2012, p. 85170P.
[16] J.D. Schmidt, Numerical Simulation of Optical Wave Propagation with Examples in Matlab, SPIE, 2010, Ch. 9.
[17] R.L. Phillips, Laser Beam Propagation Through Random Media, second ed., SPIE, 2005, Ch. 3.
[18] H. Takenaka, M. Toyoshima, Y. Takayama, Experimental verification of fiber-coupling efficiency for satellite-to-ground atmospheric laser downlinks, Opt. Express 20 (2012) 15301–15308.
[19] J. Mao, H. Sheng, C. Zhou, A fiber coupling system based on the GRIN lens for use in all-fiber lidars, J. Russ. Laser Res. 33 (2012) 186–195.
[20] J.D. Schmidt, Numerical Simulation of Optical Wave Propagation with Examples in MATLAB, SPIE, 2010, Ch. 6.
[21] K. Li, J. Ma, L. Tan, S. Yu, C. Zhai, Performance analysis of fiber-based free-space optical communications with coherent detection spatial diversity, Appl. Opt. 55 (2016) 4649–4656.
[22] Z. Wu, H. Jiang, X. Feng, S. Gao, Demonstration of cost-effective single-photodetector coherent receiver for free-space optical communications, in: Asia Communications and Photonics Conference, 2017, paper: M3G.4.
[23] A. Mecozzi, Retrieving the full optical response from amplitude data by Hilbert transform, Opt. Commun. 282 (2009) 4183–4187.
[24] M.M. Ibrahim, A.M. Ibrahim, Performance analysis of optical receivers with space diversity reception, IEE. Proc. Commun. 143 (1996) 369–372.
[25] G.K. Karagiannidis, D.A. Zogas, N.C. Sagias, S.A. Kotsopoulos, G.S. Tombras, Equal-gain and maximal-ratio combining over nonidentical weibull fading channels, IEEE Trans. Wirel. Commun. 4 (2005) 841–846.
[26] J. Ma, K. Li, L. Tan, S. Yu, Y. Cao, Performance analysis of satellite-to-ground downlink coherent optical communications with spatial diversity over Gamma-Gamma atmospheric turbulence, Appl. Opt. 54 (2015) 7575–7585.